UCLA
UCLA Previously Published Works

Title

Validation of contrast-enhanced magnetic resonance imaging to monitor regenerative efficacy after cell therapy in a porcine model of convalescent myocardial infarction.

Permalink

https://escholarship.org/uc/item/9b95b4jw

Journal

Circulation, 128(25)

ISSN

0009-7322

Authors

Malliaras, Konstantinos
Smith, Rachel R
Kanazawa, Hideaki
et al.

Publication Date

2013-12-01

DOI

10.1161/circulationaha.113.002863

Peer reviewed

eScholarship.org Powered by the California Digital Library
University of California

NIH Public Access
Author Manuscript
Circulation. Author manuscript; available in PMC 2014 December 24.

Published in final edited form as:
Circulation. 2013 December 24; 128(25): 2764–2775. doi:10.1161/CIRCULATIONAHA.113.002863.

Validation of Contrast-Enhanced MRI to Monitor Regenerative Efficacy after Cell Therapy in a Porcine Model of Convalescent Myocardial Infarction

Konstantinos Malliaras, MD[1], **Rachel R. Smith, PhD**[1,2], **Hideaki Kanazawa, MD, PhD**[1], **Kristine Yee, DVM, DACVIM**[1], **Jeffrey Seinfeld, BS**[1], **Eleni Tseliou, MD**[1], **James F. Dawkins, DVM**[1], **Michelle Kreke, PhD**[2], **Ke Cheng, PhD**[1], **Daniel Luthringer, MD**[1], **Chak-Sum Ho, PhD**[3], **Agnieszka Blusztajn, BS**[2], **Ileana Valle, BS**[2], **Supurna Chowdhury, MS**[1], **Raj R. Makkar, MD**[1], **Rohan Dharmakumar, PhD**[4], **Debiao Li, PhD**[4], **Linda Marbán, PhD**[1,2], and **Eduardo Marbán, MD, PhD**[1]

[1]Cedars-Sinai Heart Institute, Los Angeles, CA

[2]Capricor Inc., Los Angeles, CA

[3]Gift of Life Michigan, Ann Arbor, MI

[4]Cedars-Sinai Biomedical Imaging Research Institute, Los Angeles, CA

Abstract

Background—Magnetic Resonance Imaging (MRI) in the CADUCEUS trial revealed that cardiosphere-derived cells (CDCs) decrease scar size and increase viable myocardium post-myocardial infarction (MI), but MRI has not been validated as an index of regeneration after cell therapy. We tested the validity of contrast-enhanced MRI in quantifying scarred and viable myocardium after cell therapy in a porcine model of convalescent MI.

Methods and Results—Yucatan minipigs underwent induction of MI and 2-3 weeks later were randomized to receive intracoronary infusion of 12.5×10^6 mismatched allogeneic CDCs or vehicle. Allogeneic CDCs induced mild local mononuclear infiltration but no systemic immunogenicity. MRI revealed that allogeneic CDCs attenuated remodeling, improved global and regional function, decreased scar size and increased viable myocardium compared to placebo 2 months post-treatment. Extensive histological analysis validated quantitatively the MRI measurements of scar size, scar mass and viable mass. CDCs neither altered gadolinium contrast myocardial kinetics, nor induced changes in vascular density or architecture in viable and scarred myocardium. Histology demonstrated that CDCs lead to cardiomyocyte hyperplasia in the border zone, consistent with the observed stimulation of endogenous regenerative mechanisms (cardiomyocyte cycling, upregulation of endogenous progenitors, angiogenesis).

Conclusions—Contrast-enhanced MRI accurately measures scarred and viable myocardium after cell therapy in a porcine model of convalescent MI. MRI represents a useful tool for assessing dynamic changes in the infarct and monitoring regenerative efficacy.

Correspondence: Eduardo Marbán, MD Cedars-Sinai Heart Institute, 8700 Beverly Blvd., Los Angeles, CA 90048 Phone: 310-423-7557 Fax: 310-423-7637 eduardo.marban@csmc.edu..

Conflict of Interest Disclosures: EM and LM own equity in Capricor, Inc. KM is a consultant for Capricor, Inc. Other authors have no relationships to disclose.

NIH-PA Author Manuscript
NIH-PA Author Manuscript
NIH-PA Author Manuscript

NIH-PA Author Manuscript

NIH-PA Author Manuscript

NIH-PA Author Manuscript

Keywords

allogeneic transplantation; cardiosphere-derived cells; heart regeneration; magnetic resonance imaging

Cell therapy has emerged as a potential therapeutic strategy for ischemic cardiomyopathy. While the paradigm of administering bone marrow-derived cells in the setting of acute or recent myocardial infarctions (MIs) has proven to be safe, efficacy has been inconsistent[1,2]. Early clinical experience with autologous heart-derived progenitor cells has been more encouraging[3,4]. In the CADUCEUS trial, intracoronary infusion of autologous cardiosphere-derived cells (CDCs)[5] in post-MI patients with left ventricular (LV) dysfunction decreased scar size, increased viable myocardium and improved regional function, as measured by contrast-enhanced magnetic resonance imaging (MRI)[3]. Contrast-enhanced MRI has been extensively validated (and is considered the "gold standard" imaging modality) for the quantification of necrotic/scarred and viable myocardium in the setting of acute or chronic MI[6-8]. Thus, MRI represents a potentially useful tool for monitoring regenerative efficacy, as it affords the unique ability to quantify, rigorously and independently, scar mass and viable myocardial mass in human subjects before and after cell therapy interventions[9]. However, its validity in characterizing tissue viability after cell administration has been called into question[10]. Without evidence, concerns have been raised that cell therapy may promote changes in vessel density or architecture (e.g., increase in wall thickness or decrease in vascular permeability) that could affect gadolinium (Gd)-contrast myocardial kinetics (in the form of accelerated contrast wash-out [a phenomenon that has been described in non-cardiac tissues[11]] or decreased contrast extravasation, respectively), therefore compromising the ability of contrast-enhanced MRI to distinguish scar from viable myocardium[10].

Here, we sought to test the validity of contrast-enhanced MRI to distinguish, and accurately measure, scarred and viable myocardium after cell therapy. We used a porcine model of intracoronary infusion of allogeneic CDCs, which enabled us to concurrently investigate the safety and efficacy of allogeneic heart-derived cells without immunosuppression in a clinically-relevant model of convalescent MI.

METHODS

All animal studies were performed in an American Association for Accreditation of Laboratory Animal Care accredited facility with approval from the Institutional Animal Care and Use Committee of the Cedars-Sinai Medical Center (IACUC 3661). The experimental protocol is depicted schematically in Figure 1. A total of 26 minipigs were studied: 3 completed the 24-hour retention study (Fig 1A), 10 completed the validation study (Fig 1B), 5 completed the 2-month engraftment study, 4 were excluded per protocol for procedural mortality, 3 were used for allosensitization protocols, and 1 served as CDC donor.

Cell culture

Allogeneic CDCs were grown from a freshly-explanted heart obtained from one male Sinclair minipig (Sinclair Bioresources) (for detailed methods see Online Supplement). For 24-hour retention analysis, CDCs were transduced with an adenoviral vector carrying the firefly luciferase gene 3 days prior to infusion.

NIH-PA Author Manuscript

NIH-PA Author Manuscript

NIH-PA Author Manuscript

MI creation and CDC infusion

Infarcts were created in adult Yucatan minipigs by inflation of an angioplasty balloon in the mid-left anterior descending artery (LAD) (distal to the 1st diagonal branch) for 2.5 h (for detailed methods see Online Supplement). Two to 3 weeks later, pigs were randomized to receive 12.5 million CDCs (in 10 mls of Cryostor™CS10 containing 45 μg/ml nitroglycerin and 180 U/ml heparin) or vehicle. Intracoronary infusion was performed via an over-the-wire balloon catheter, placed in the mid-LAD. CDCs or vehicle solution were infused in 3 cycles of intermittent balloon inflation[12]. Minipigs were euthanized either 24 hours post-infusion, to measure short-term cardiac retention of administered cells (n=3), or 2 months later (n=15; 10 completed the validation study, 5 completed the 2-month engraftment study).

In vivo cardiac MRI

Baseline (2-3 weeks post-MI, before intracoronary infusion) and endpoint (2 months post-infusion) contrast-enhanced cardiac MRI was performed to measure scar mass, viable myocardial mass (i.e., total mass minus scar mass), scar size (scar mass divided by total mass), volumes, global function, and regional function of the LV.

All MRI studies were performed on a 3.0 T clinical MRI scanner (Siemens MAGNETOM Verio®, Erlangen, Germany). Typical in-plane resolution was 1.3 × 1.3 mm, and slice thickness was 6 mm, with no gaps. Global LV function, regional systolic thickening and regional end-systolic thickness were assessed using ECG-gated and breath-held cine steady-state free precession acquisitions[13]. Minipigs undergoing baseline MRI subsequently received an IV injection of Gd-based contrast agent gadoversetamide (OptiMARK®, Covidien Imaging Solutions, Hazelwood, MO, USA; 0.2 mmol/kg body weight), and, 8 minutes later, delayed contrast-enhanced images were acquired with an ECG-gated, breath-hold, interleaved, 2D-Turbo FLASH sequence[14]. The inversion time was adjusted by the scanner operator to null signal from non-infarcted remote myocardium.

In minipigs undergoing endpoint MRI, once the cine acquisitions were completed, a short-axis slice with significant regional hypokinesia was selected (after review of cine images) to study Gd-contrast kinetics. Minipigs received an IV injection of Gd-contrast (0.1 mmol/kg body weight) and a series of dynamic delayed contrast enhancement images were acquired (pre– and 1, 2, 3, 4, 5, 6, 10, 12, 14, 16, 18 and 20 minutes post-contrast administration). An ECG-gated, breath-hold, interleaved 2D-Turbo FLASH sequence was used, and the inversion time was kept constant at 270 ms[15,16]. Thirty minutes after the first contrast injection, a TI scout was performed to ensure sufficient contrast clearance. Subsequently, minipigs received a second IV injection of Gd-contrast (0.2 mmol/kg body weight) and 8 minutes later delayed contrast-enhanced images were acquired to assess scar size as described above for baseline MRI. Thirty minutes after the second contrast injection, a TI scout was performed to ensure sufficient contrast clearance. Subsequently, minipigs received a third IV injection of Gd-contrast (0.2 mmol/kg body weight) and were sacrificed 15 minutes later in order to perform ex vivo MRI of the heart.

All image analyses were performed using validated image processing software (QMass MR®, Medis medical imaging systems). Global function and cardiac volumes were evaluated by a researcher blinded to treatment allocation. To evaluate regional function, each short-axis slice was divided into 6 segments, using the right ventricular insertion as a reference point. Scar size from late Gd-enhanced cardiac MR images was defined based on the full-width half-max (FWHM) criterion to delineate scarred myocardium[7].

NIH-PA Author Manuscript

NIH-PA Author Manuscript

NIH-PA Author Manuscript

Ex vivo cardiac MRI & histology

Hearts from minipigs sacrificed 2 months post- infusion underwent ex vivo MRI. The heart was removed ~30 minutes post Gd-DTPA administration, thoroughly rinsed in ice-cold saline to remove any residual blood, and suspended by sutures in a plastic container filled with saline. 3D Turbo FLASH images were acquired with a resolution of 1 × 1 × 1 mm ^{6}. After image acquisition, the heart was sectioned into 1 cm thick short-axis slices, which were incubated with 2% 2,3,5-triphenyltetrazolium chloride (TTC) for 20 min at 37°C to stain viable myocardium. Each slice was photographed with a digital camera and infarct size was determined as the percentage of LV volume by manual tracing by a researcher blinded to treatment allocation (ImageJ, version 1.46, National Institutes of Health, Bethesda, MA, USA). Scar and viable myocardium volumes were calculated by multiplying scar and viable area for each slice (in mm^2) with the corresponding slice thickness. Scar mass and viable myocardial mass were calculated by multiplying the scar and viable myocardial volumes times a specific gravity of 1.05g/cm^3.

Immune rejection in the heart was investigated by hematoxylin and eosin staining; analysis was performed by an experienced cardiac pathologist blinded to treatment allocation (DL), and rejection was graded according to the International Society for Heart & Lung Transplantation (ISHLT) grading system, used in clinical practice to diagnose solid organ transplant rejection. Morphometric analysis was performed with Masson's trichrome staining. Vascular density and architecture were investigated by fluorescent immunohistochemistry; arterioles and arteries were defined as smooth-muscle-coated vessels with external vascular diameter (lumen + vascular walls) <75 μm and >75μm respectively. Myocyte cross-sectional area was investigated by fluorescent immunohistochemistry; cardiomyocytes were accepted for size measurement if they met the following criteria: (a) cellular cross-sections present (b) visible nuclei located close to the cell center and (c) intact cell borders[17]. Cardiomyocyte cell-cycling and activation of cardiac progenitors were investigated by fluorescent immunohistochemistry. In all histological analyses, peri-infarct (border zone) area was defined as the region at the edges of the scar (comprising areas of both viable and scarred myocardium). For detailed histological methods see the Online Supplement.

Evaluation of 24-hour cardiac retention and 2-month cardiac engraftment

Evaluation of 24-hour cardiac retention was performed with the ex vivo luciferase assay[12] (Supp Fig 1a; for details see the Online Supplement). Two-month cardiac engraftment was investigated by Fluorescence In Situ Hydridization (FISH) for the male Y chromosome (Supp Fig 2) 2 months after sex-mismatch cell transplantation (male cells infused into infarcted female recipients; for details see the Online Supplement).

Histocompatibility

To assess histocompatibility, low-resolution swine leukocyte antigen (SLA) typing was performed on the donor and recipient minipigs as described in the Online Supplement.

Circulating donor-specific antibodies

To evaluate humoral immune response, recipient minipig serum samples (obtained at baseline, 1 day, 1 week, 2 weeks and 2 months post-infusion) were screened for circulating anti-donor IgG antibodies by flow cytometry[18].

An allosensitization protocol was performed to provide positive controls for the flow cytometry assay. Peripheral bone marrow mononuclear cells (PBMNCs) were harvested from a donor farm pig and injected intradermally and subcutaneously into the pinnae of

NIH-PA Author Manuscript

NIH-PA Author Manuscript

NIH-PA Author Manuscript

recipient Yucatan minipigs (n=2, 190 million PBMNCs injected per pig). Serum samples collected 2 weeks post PBMNC injection served as positive controls for allosensitization.

Statistical Analysis

Results are presented as mean ± SD in the text and as mean ± SEM in the figures. For continuous measures, differences between 2 groups (controls, CDC-treated) were tested using independent samples t-test. Comparisons of changes from baseline within groups were performed using paired samples t-test. Histology data for grading of rejection were analyzed using a generalized estimating equations (GEE) logistic regression model. Gd curves were analyzed with a linear mixed effects model using random intercept to control for repeated measures and Tukey's adjustment for multiple comparisons. Serial Troponin I (TnI) measurements were analyzed using a GEE model with an autoregressive correlation structure. Pearson correlations and the Bland-Altman analysis method were used to compare MRI measurements against postmortem histological measurements. All tests were 2-sided. No multiplicity adjustment for multiple comparisons was performed. A p value of <0.05 was considered statistically significant.

RESULTS

Safety of CDC infusion, 24-hour retention and 2-month engraftment

Four of 22 minipigs (18%) died during creation of MI due to ventricular arrhythmias. There was no further mortality (0%) in minipigs that survived the MI.

CDCs are ~20μm in diameter, so that microvascular occlusion is expected at escalating doses[12]. We thus looked for any infusion-related impairment of coronary flow or increase in ischemic biomarkers. No adverse events (sustained ventricular arrhythmias, unresolved ST-segment elevations) occurred during cell infusion, and no impairment of TIMI flow was observed after infusion (Supp Fig 3b). No difference in serum TnI was detected between the CDC-treated and placebo groups at 1,7,14, or 60 days post-infusion (Supp Fig 3A). The mild TnI elevations observed 1 day post-infusion in both groups are consistent with transient LAD occlusion by the stop-flow infusion procedure.

To assess short-term cardiac retention of infused CDCs, 3 minipigs were infused with luciferase-labeled allogeneic CDCs. Twenty-four hours later, the ex vivo luciferase assay (Supp Fig 1A) revealed that cardiac retention of CDCs was 4.3±2.2% (Supp Fig 1B). Long-term cardiac engraftment was investigated by FISH for the male Y chromosome (after infusion of male CDCs into female recipients). While presence of infused cells in the recipient myocardium could be verified at 2 weeks post-infusion (Supp Fig 2), no allogeneic (male) cells could be detected at 2 months post-infusion (5 animals, 4782 nuclei analyzed)

Immune reaction to allogeneic CDCs

Low-resolution SLA genotyping revealed complete Class I (SLA-1, SLA-2, SLA-3) and Class II (DRB1, DQB1, DQA) mismatches between the donor minipig and CDC recipients (Supp Fig 4). Cardiac histology demonstrated a marginally significant increase in focal lymphoplasmacytic infiltration (deemed to be unrelated to the natural inflammatory response to the ischemic insult) in the peri-infarct area of CDC-treated minipigs compared to placebo ($p=0.058$ between groups, Odds Ratio=8.61 [95% CI: 0.93-79.52]). (Supp Fig 5A). The infiltrating cells were localized within interstitial and perivascular spaces (Grade 1R according to the ISHLT grading system) (Supp Fig 5B); importantly, no foci of rejection-associated myocyte damage were detected. The remote myocardium was consistently clear of inflammatory infiltrates. No circulating alloreactive antibodies were detected in any recipients of allogeneic CDCs at any time point. In contrast, in minipigs that were

NIH-PA Author Manuscript

NIH-PA Author Manuscript

NIH-PA Author Manuscript

allosensitized by intradermal and subcutaneous PBMNC injections, high titers of circulating alloreactive IgG antibodies were detected 2 weeks post-injection (Supp Figure 5C,D).

Functional and structural benefits after infusion of allogeneic CDCs

To assess efficacy of allogeneic CDCs, minipigs underwent cardiac MRI before infusion (2-3 weeks post MI) and 2 months later. Allogeneic CDCs resulted in preservation of LVEF (Δ:−0.5±3.2, p=0.73 within group), while LVEF decreased in control animals (Δ:−9.9±1.3%, p<0.001 within group, p<0.001 between groups) (Fig 2A-C, Supplemental Videos 1-4). In addition, allogeneic CDCs attenuated LV remodeling: CDC-treated animals exhibited a smaller increase in ESV (Δ:10.9±7.4ml) compared to controls (Δ:26.6±13.2ml, p=0.048 between groups) (Fig 2E). EDV increased in both CDC-treated animals (Δ:17.7±10.5ml, p=0.020 within group) and controls (Δ:30.5±19.8ml, p=0.026 within group, p=0.24 between groups) (Fig 2D).

Regional function was assessed in infarcted and non-infarcted myocardial segments, after visual inspection of corresponding late Gd-enhanced images. Two months post-infusion, CDC-treated infarcted myocardial segments displayed increased systolic thickening (p<0.001 between groups), and increased end-systolic thickness (p=0.025 between groups), compared to infarcted segments from placebo-treated animals (Fig 2F,G). In addition, regional function in the non-infarcted myocardial segments was improved in CDC-treated animals compared to controls, consistent with attenuation of LV remodeling (Fig 2F,G).

Fig. 3A shows representative late Gd-enhanced MRI acquisitions of hearts in short-axis section at end-diastole. Gd-contrast agent accumulates in the infarct scar (as a result of a larger distribution volume due to increased extracellular space in the scar compared with normal myocardium[19,20]). In the CDC-treated minipig, the infarcted wall thickness was preserved 2 months post-infusion; importantly, the scar decreased in transmurality, while viable myocardial mass increased. In contrast, the placebo-treated minipig was characterized by infarct thinning and expansion, with no evidence of an increase in viable myocardium over the same time period (Fig. 3A).

Two months post-infusion, MRI analysis revealed that scar size remained unchanged in controls (Δ:0.4±0.9%, p=0.33 within group) but decreased in CDC-treated animals (Δ: −3.6 ±2.4%, p=0.026 within group, p=0.007 between groups) (Fig 3B), resulting in significantly smaller scar size in CDC-treated animals (9.2±0.8%) compared to controls (14.6±3.2%, p=0.006 between groups), despite similar scar size at baseline (12.8±2.8% [CDCs] vs 14.1±2.8% [controls], p=0.48 between groups) (Fig 3E). While scar size is a conventional measure of myocardial viability, cardiac MRI can quantify independently the individual components of scar mass and viable myocardial mass[9], enabling more discriminating insight into mechanism. Scar mass decreased in CDC-treated animals (Δ:−1.4±1.4g), but not in controls (Δ:0.8±0.6g, p=0.012 between groups) (Fig 3C), resulting in a trend towards smaller endpoint scar mass in CDC-treated animals (6.6±0.7g) compared to controls (9.7.3±3.5g, p:0.093 between groups) (Fig 3F). In addition, CDC-treated animals exhibited significant increases in viable myocardial mass (Δ:10.7±3.6g) compared to controls (Δ: 2.7±2.1g, p=0.003 between groups) over 2 months (Fig 3D), resulting in greater endpoint viable mass (65.8.9±4.5g) compared to controls (55.5±5.0g, p=0.010 between groups) (Fig 3G). A complete list of MRI-measured parameters for each experimental animal is provided in Supp Table 1.

NIH-PA Author Manuscript

NIH-PA Author Manuscript

NIH-PA Author Manuscript

Comparison of cardiac MRI with histology for assessment of scarred and viable myocardium after cell therapy

Post-mortem histological analysis confirmed the MRI results, not just qualitatively but also with quantitative accuracy. Fig 4A shows representative short-axis cardiac slices after incubation with TTC, while Fig 4B shows representative sections from the infarcted wall stained with Masson's trichrome. CDC-treated hearts consistently exhibited significant amounts of viable myocardium in the infarcted wall, most often in the form of endocardial and epicardial muscular layers surrounding the scar but also in the form of islets of viable myocardial tissue interspersed between the collagen fibers. In contrast, in control minipigs the scar was homogeneous and largely transmural (Fig 4A,B,F). The increased amount of viable myocardium in the infarct region after cell therapy is consistent with the improved regional contractility of infarcted segments in CDC-treated animals compared to controls (Fig 2F,G). Histological measurement of scar and viable myocardium demonstrated decreased scar transmurality in CDC-treated animals (44.1±21.3% vs 79.3±25.2%, p=0.044), smaller scar size (9.1±1.2% vs 14.0±2.9%, p=0.009) and increased viable myocardial mass (68.7±4.7g vs 55.2±4.9g, p=0.002) in CDC-treated animals compared to infarcted controls (Fig 4C-F), yielding virtually identical results to those obtained from contrast-enhanced MRI (Fig 3E-G). A complete list of histological measurements of scar size, scar mass and viable mass for each experimental animal is provided in Supp Table 2. To further evaluate the ability of contrast-enhanced MRI to accurately measure scarred and viable myocardium after cell therapy, all TTC-stained cardiac slices were matched with their corresponding late Gd-enhanced images (from both the in vivo and ex vivo MRI datasets). Fig 5A provides representative examples of this analysis for a CDC-treated and a control minipig. In both cases, areas of hyperenhancement in cardiac MRIs correspond faithfully to regions of scarred myocardium in histological slices. Importantly, MRI reveals significant amounts of viable myocardium within the infarct region of the CDC-treated heart, a finding that is confirmed by cardiac histology: the endocardial and epicardial rims of non-hyperenhanced tissue in the infarcted wall in contrast-enhanced MRIs are virtually identical to the endocardial and epicardial TTC-positive muscular layers surrounding the scar in histological slices. In contrast, the control heart is characterized by a dense transmural scar, and no viable myocardium can be detected in the infarct area by either MRI or histology. Figs 5B-D show quantitative correlation analysis between the various MRI parameters and the corresponding histological values; the measures of scar size (as % of isolated cardiac slices and as % of the LV), LV scar mass and LV viable mass all correlate strongly, with a slope close to the line of identity. Bland-Altman analysis demonstrated excellent agreement between MRI and post-mortem histology (Supp Fig 6).

MR imaging of Gd-contrast kinetics in cell-treated myocardium

To assess whether cell therapy fundamentally alters myocardial contrast uptake and/or wash-out, we compared Gd-contrast kinetics in various regions infused with cells to the kinetics in the remote (non-infarcted, non-cell treated) myocardium. A series of dynamic late Gd-enhanced images were acquired with a fixed TI (Fig 6A)[15,16], and signal intensity of specific areas (collagenous scar, viable myocardium in the infarcted region, viable myocardium at the border zone, remote myocardium) was measured at various timepoints following contrast administration, resulting in the generation of site-specific Gd-contrast curves (Fig 6B; pooled data from all CDC-treated minipigs). Analysis using a linear mixed effects model demonstrated that the only site in which Gd kinetics were (predictably) different compared to remote healthy myocardium was the infarct scar. Importantly, Gd-contrast kinetics were virtually identical in cell-treated viable (non-hyperenhanced) areas and in the remote non-cell treated healthy myocardium.

NIH-PA Author Manuscript

NIH-PA Author Manuscript

NIH-PA Author Manuscript

Vascular density and architecture

To investigate whether cell therapy with CDCs can induce vascular changes in the treated (scarred or viable) myocardium, we studied vessel density and architecture in the collagenous scar, in viable myocardium in the infarcted wall and in the remote (non-infarcted, non-cell treated) myocardium. As expected[21,22], capillary density was low in the collagenous scar (117.7±32.9 vessels/mm^2) and in the border zone (525.3±274.3 vessels/mm^2) as compared to remote myocardium (1344.4±356.5 vessels/mm^2). While total capillary density was increased in the border zone (defined as the region at the edges of the scar comprising areas of both scarred and viable myocardium) of CDC-treated hearts (721.9±192.5 vessels/mm^2 vs 328.8±188.8 vessels/mm^2, p=0.012) (Fig 7B), no differences in capillary, arteriolar or arterial density in scarred or viable myocardium could be detected between CDC-treated animals and controls (Fig 7C). Thus, the increased total capillary density in the border zone of CDC-treated hearts is a result of the increased viable mass and decreased scar mass observed in the infarct border zone after CDC therapy, and cannot be attributed to differences in vascular density of scarred or viable myocardium between CDC-treated hearts and controls. Vessel architecture (as quantified by lumen diameter [Fig 7D], wall thickness, endothelial layer thickness, smooth muscle layer thickness [Fig 7E] and lumen/wall ratio [7F]) was similar in CDC-treated and control hearts.

Stimulation of endogenous cardiac regeneration by allogeneic CDCs

To investigate whether the increased viable myocardium observed after CDC-therapy was a result of myocyte hypertrophy, we measured cardiomyocyte cross-sectional area in the infarct and peri-infarct area. Myocyte size was significantly smaller in CDC-treated animals compared to controls (Fig 8A), thus excluding myocyte hypertrophy as a contributor to the increase in viable myocardium. The conjunction of increased viable mass and smaller myocyte size are indicative of cardiomyocyte hyperplasia after cell therapy. With regard to the latter, we found that transplantation of CDCs upregulated cardiomyocyte cycling (Fig 8B) and increased the number of small round TnI+ cells (previously defined as putative myocyte progenitors[22,23]) in the infarct and peri-infarct area (Fig 8C), confirming previous reports[18,24]. While cardiomyogenesis is likely to play a role in the reduction of cardiomyocyte area, attenuation of adverse remodeling (which involves cardiomyocyte hypertrophy) may potentiate the reduction in myocyte size in the infarct and peri-infarct area of CDC-treated animals. Supporting this conjecture, myocyte cross-sectional area in the remote myocardium tended to be lower as well (consistent with relief of wall stress), although the differences did not reach statistical significance (Supp Fig 7).

DISCUSSION

Heart-derived cells are particularly promising for cardiac repair and regeneration. In the CADUCEUS trial, intracoronary infusion of autologous CDCs decreased scar size, increased viable myocardium and improved regional myocardial function, as measured by MRI[3]. An interim MRI analysis of the still-ongoing SCIPIO trial (where MRI was performed only in treated, primarily non-randomized patients) showed similar results[4]. Although late Gd-enhanced cardiac MRI has been extensively validated for the quantification of necrotic/fibrotic and viable myocardium in acute/chronic MI[6-8], its validity to accurately characterize tissue viability after cell therapy has been questioned[10]: cell administration may increase vascular wall thickness, resulting in decreased vessel permeability and attenuation of Gd-contrast extravasation in cell-treated myocardial regions, or stimulate angiogenesis, leading to enhanced drainage of Gd-contrast from the cell-treated myocardium (a phenomenon that has been described in hypervascular hepatocellular carcinomas[11]). Any of these confounding factors, if operative, would result in altered Gd-

NIH-PA Author Manuscript

NIH-PA Author Manuscript

NIH-PA Author Manuscript

contrast myocardial kinetics (in the form of decreased contrast extravasation or accelerated wash-out) that could compromise the fidelity of contrast-enhanced MRI[10].

We sought to validate experimentally the ability of contrast-enhanced MRI to distinguish and accurately measure scarred from viable myocardium after cell therapy. We find that CDC infusion does not change vascular density or architecture in scarred and viable myocardium, neither does it result in altered Gd-contrast myocardial tissue kinetics. Importantly, using post-mortem histology as the gold standard, we demonstrate that contrast-enhanced MRI readily distinguishes viable and scarred myocardium and provides accurate measurements of scar size, scar mass and viable myocardial mass in cell-treated hearts.

The present work differs from previous human[3] and porcine[12] studies of CDCs in that the prior studies used autologous cells. The effects of allogeneic CDC therapy reported here are qualitatively similar, and at least as impressive quantitatively in terms of regenerative and functional efficacy; however, a head-to-head comparison of allogeneic versus autologous cells was beyond the scope of this study. The greater increase in EF observed in this study may be attributable to one of several factors: 1) increased efficacy of allogeneic cells (not evident in previous rat studies, which showed equivalence of intramyocardially-injected allogeneic and syngeneic CDCs[18] or cardiospheres[25]); 2) the earlier administration of CDCs here (2-3 weeks post-MI, versus 4-5 weeks in our autologous porcine study[12] or 1.5-3 months post-MI in humans[3]). A comparison of EF values in the present study versus our previous porcine study[12] reveals higher baseline EF values in both groups (a finding consistent with the earlier timepoint of baseline imaging) and a larger decrease in EF in the control group over the period of 2 months in the present study; EF of the treated group is preserved over time in both studies. These data may hint that administration of CDCs earlier in the remodeling process may offer increased functional benefit; and 3) the absence of concomitant anti-remodeling therapies (which in the human setting leave little room for EF improvement). Allogeneic CDCs induced a mild local immune reaction in the heart with no signs of immune-related myocardial damage. Importantly, no circulating anti-donor antibodies could be detected, predicting that no development of panel reactive antibodies would occur in the human setting (at least after a single administration of allogeneic cells). The efficacy of allogeneic cells is rationalized by their indirect mechanism of benefit[18], which relies on activation of endogenous reparative and regenerative pathways (increased cardiomyocyte cycling, upregulation of endogenous progenitors, angiogenesis), rather than long-term engraftment and differentiation of transplanted cells (no donor cells could be detected in the recipient myocardium 2 months post-administration).

While cardiac MRI cannot distinguish cardiac hypertrophy from hyperplasia, post-mortem histological analysis ruled out myocyte hypertrophy as a contributor to the increase in viable myocardium observed after CDC therapy; myocyte size was actually smaller in the infarct and peri-infarct area of CDC-treated animals compared to controls, a finding consistent with attenuation of remodeling-associated cardiomyocyte hypertrophy and birth of new (smaller) myocytes after cell therapy. The latter likely occurs through differentiation of endogenous progenitors (visualized here as small round TnI+ cells) and induction of resident cardiomyocyte proliferation in the border zone, in agreement with results from fate-mapping studies[24].

LIMITATIONS

Our study has several limitations. First, delayed contrast enhancement images were acquired 8 minutes post-Gd administration. Even though the FWHM technique (used here) has been shown to provide accurate measurement of infarct size as early as 6 minutes post contrast

NIH-PA Author Manuscript

NIH-PA Author Manuscript

NIH-PA Author Manuscript

administration[7], standardized protocols issued by the Society for Cardiovascular Magnetic Resonance advocate waiting at least 10 minutes[26] before acquisition of delayed contrast enhancement images. Second, allogeneic CDCs were derived from a single healthy donor minipig; we did not investigate inter-donor variability in cell immunogenicity or potency. Finally, we did not investigate the safety and efficacy of repeat administrations of allogeneic CDCs. Careful preclinical studies of safety and efficacy will be required before repeat dosing with allogeneic cells can be contemplated.

CONCLUSIONS

In conclusion, we validate the ability of late Gd enhancement MRI to accurately measure scarred and viable myocardium after cell therapy, supporting the utility of contrast-enhanced MRI for assessing dynamic changes in the infarct and monitoring therapeutic regenerative efficacy. We also demonstrate that intracoronary infusion of allogeneic CDCs without immunosuppression is safe, improves heart function and indirectly promotes cardiac regeneration in a clinically-relevant porcine model of convalescent MI. The safety and efficacy of allogeneic CDCs in human subjects with LV dysfunction post-MI is currently being tested in the phase 1/2 randomized double-blind, placebo-controlled ALLSTAR trial, (ALLogeneic heart STem Cells to achieve myocArdial Regeneration, NCT01458405)[27], which uses infarct size assessed by MRI as its primary efficacy endpoint.

Supplementary Material

Refer to Web version on PubMed Central for supplementary material.

Acknowledgments

We thank Adrian Glenn, Hao Zeng, Miguel Huerta, Claudia Anchante, Julie Avalos and Stephen Taylor for their technical and surgical support, Laura Smith for performing the MRI scans and analyzing MRIs, Nina Duong for blood processing, and David Elashoff and Tristan Grogan for statistical consulting.

Funding Sources: This work was supported by a grant to RRS from the NIH (HL103356), and by a grant to EM from the California Institute for Regenerative Medicine. Statistical analysis was supported by NIH/National Center for Advancing Translational Science (NCATS) UCLA CTSI Grant Number UL1TR000124.General laboratory support was provided by the Cedars-Sinai Board of Governors Heart Stem Cell Center.

References

1. Dauwe DF, Janssens SP. Stem cell therapy for the treatment of myocardial infarction. Curr Pharm Des. 2011; 17:3328–3340. [PubMed: 21919877]
2. Malliaras K, Marbán E. Cardiac cell therapy: where we've been, where we are, and where we should be headed. Br Med Bull. 2011; 98:161–185. [PubMed: 21652595]
3. Makkar RR, Smith RR, Cheng K, Malliaras K, Thomson LE, Berman D, Czer LS, Marbán L, Mendizabal A, Johnston PV, Russell SD, Schuleri KH, Lardo AC, Gerstenblith G, Marbán E. Intracoronary cardiosphere-derived cells for heart regeneration after myocardial infarction (CADUCEUS): a prospective, randomised phase 1 trial. Lancet. 2012; 379:895–904. [PubMed: 22336189]
4. Chugh AR, Beache GM, Loughran JH, Mewton N, Elmore JB, Kajstura J, Pappas P, Tatooles A, Stoddard MF, Lima JA, Slaughter MS, Anversa P, Bolli R. Administration of cardiac stem cells in patients with ischemic cardiomyopathy: the SCIPIO trial: surgical aspects and interim analysis of myocardial function and viability by magnetic resonance. Circulation. 2012; 126(11 Suppl 1):S54–64. [PubMed: 22965994]
5. Smith RR, Barile L, Cho HC, Leppo MK, Hare JM, Messina E, Giacomello A, Abraham MR, Marbán E. Regenerative potential of cardiosphere-derived cells expanded from percutaneous endomyocardial biopsy specimens. Circulation. 2007; 115:896–908. [PubMed: 17283259]

NIH-PA Author Manuscript

NIH-PA Author Manuscript

NIH-PA Author Manuscript

6. Kim RJ, Fieno DS, Parrish TB, Harris K, Chen EL, Simonetti O, Bundy J, Finn JP, Klocke FJ, Judd RM. Relationship of MRI delayed contrast enhancement to irreversible injury, infarct age, and contractile function. Circulation. 1999; 100:1992–2002. [PubMed: 10556226]
7. Amado LC, Gerber BL, Gupta SN, Rettmann DW, Szarf G, Schock R, Nasir K, Kraitchman DL, Lima JA. Accurate and objective infarct sizing by contrast enhanced magnetic resonance imaging in a canine myocardial infarction model. J Am Coll Cardiol. 2004; 44:2383–2389. [PubMed: 15607402]
8. Schelbert EB, Hsu LY, Anderson SA, Mohanty BD, Karim SM, Kellman P, Aletras AH, Arai AE. Late gadolinium-enhancement cardiac magnetic resonance identifies postinfarction myocardial fibrosis and the border zone at the near cellular level in ex vivo rat heart. Circ Cardiovasc Imaging. 2010; 3:743–752. [PubMed: 20847191]
9. Malliaras K, Kreke M, Marbán E. The stuttering progress of cell therapy for heart disease. Clin Pharmacol Ther. 2011; 90:532–541. [PubMed: 21900888]
10. Chin MT, Murry CE. Is it possible to transform cardiac scar tissue into beating heart muscle in humans? Regen Med. 2012; 7:623–625. [PubMed: 22954430]
11. Yu JS, Chung JJ, Kim JH, Kim KW. Small hypervascular hepatocellular carcinomas: value of “washout” on gadolinium-enhanced dynamic MR imaging compared to superparamagnetic iron oxide-enhanced imaging. Eur Radiol. 2009; 19:2614–2622. [PubMed: 19513719]
12. Johnston PV, Sasano T, Mills K, Evers R, Lee ST, Smith RR, Lardo AC, Lai S, Steenbergen C, Gerstenblith G, Lange R, Marbán E. Engraftment, differentiation, and functional benefits of autologous cardiosphere-derived cells in porcine ischemic cardiomyopathy. Circulation. 2009; 120:1075–1083. [PubMed: 19738142]
13. Carr JC, Simonetti O, Bundy J, Li D, Pereles S, Finn JP. Cine MR angiography of the heart with segmented true fast imaging with steady-state precession. Radiology. 2001; 219:828–834. [PubMed: 11376278]
14. Simonetti OP, Kim RJ, Fieno DS, Hillenbrand HB, Wu E, Bundy JM, Finn JP, Judd RM. An improved MR imaging technique for the visualization of myocardial infarction. Radiology. 2001; 218:215–223. [PubMed: 11152805]
15. Wagner A, Mahrholdt H, Thomson L, Hager S, Meinhardt G, Rehwald W, Parker M, Shah D, Sechtem U, Kim RJ, Judd RM. Effects of time, dose, and inversion time for acute myocardial infarct size measurements based on magnetic resonance imaging-delayed contrast enhancement. J Am Coll Cardiol. 2006; 47:2027–2033. [PubMed: 16697321]
16. Knowles BR, Batchelor PG, Parish V, Ginks M, Plein S, Razavi R, Schaeffter T. Pharmacokinetic modeling of delayed gadolinium enhancement in the myocardium. Magn Reson Med. 2008; 60:1524–30. [PubMed: 19025896]
17. Drakos SG, Kfoury AG, Hammond EH, Reid BB, Revelo MP, Rasmusson BY, Whitehead KJ, Salama ME, Selzman CH, Stehlik J, Clayson SE, Bristow MR, Renlund DG, Li DY. Impact of mechanical unloading on microvasculature and associated central remodeling features of the failing human heart. J Am Coll Cardiol. 2010; 56:382–391. [PubMed: 20650360]
18. Malliaras K, Li TS, Luthringer D, Terrovitis J, Cheng K, Chakravarty T, Galang G, Zhang Y, Schoenhoff F, Van Eyk J, Marbán L, Marbán E. Safety and efficacy of allogeneic cell therapy in infarcted rats transplanted with mismatched cardiosphere-derived cells. Circulation. 2012; 125:100–112. [PubMed: 22086878]
19. Ordovas KG, Higgins CB. Delayed contrast enhancement on MR images of myocardium: past, present, future. Radiology. 2011; 261:358–374. [PubMed: 22012903]
20. Arai AE. The cardiac magnetic resonance (CMR) approach to assessing myocardial viability. J Nucl Cardiol. 2011; 18:1095–1102. [PubMed: 21882082]
21. Dubois C, Liu X, Claus P, Marsboom G, Pokreisz P, Vandenwijngaert S, Dépelteau H, Streb W, Chaothawee L, Maes F, Gheysens O, Debyser Z, Gillijns H, Pellens M, Vandendriessche T, Chuah M, Collen D, Verbeken E, Belmans A, Van de Werf F, Bogaert J, Janssens S. Differential effects of progenitor cell populations on left ventricular remodeling and myocardial neovascularization after myocardial infarction. J Am Coll Cardiol. 2010; 55:2232–2243. [PubMed: 20466204]

NIH-PA Author Manuscript

NIH-PA Author Manuscript

NIH-PA Author Manuscript

22. Lin YD, Luo CY, Hu YN, Yeh ML, Hsueh YC, Chang MY, Tsai DC, Wang JN, Tang MJ, Wei EI, Springer ML, Hsieh PC. Instructive nanofiber scaffolds with VEGF create a microenvironment for arteriogenesis and cardiac repair. Sci Transl Med. 2012; 4:146ra109. 8.

23. Davis ME, Motion JP, Narmoneva DA, Takahashi T, Hakuno D, Kamm RD, Zhang S, Lee RT. Injectable self-assembling peptide nanofibers create intramyocardial microenvironments for endothelial cells. Circulation. 2005; 111:442–450. [PubMed: 15687132]

24. Malliaras K, Zhang Y, Seinfeld J, Galang G, Tseliou E, Cheng K, Sun B, Aminzadeh M, Marbán E. Cardiomyocyte proliferation and progenitor cell recruitment underlie therapeutic regeneration after myocardial infarction in the adult mouse heart. EMBO Mol Med. 2013; 5:191–209. [PubMed: 23255322]

25. Tseliou E, Pollan S, Malliaras K, Terrovitis J, Sun B, Galang G, Marbán L, Luthringer D, Marbán E. Allogeneic cardiospheres safely boost cardiac function and attenuate adverse remodeling post-myocardial infarction in immunologically-mismatched rat strains. J Am Coll Cardiol. 2013; 61:1108–1119. [PubMed: 23352785]

26. Kramer CM, Barkhausen J, Flamm SD, Kim RJ, Nagel E. Society for Cardiovascular Magnetic Resonance Board of Trustees Task Force on Standardized Protocols. Standardized cardiovascular magnetic resonance imaging (CMR) protocols, society for cardiovascular magnetic resonance: board of trustees task force on standardized protocols. J Cardiovasc Magn Reson. 2008; 10:35. [PubMed: 18605997]

27. [February 28, 2013] Allogeneic Heart Stem Cells to Achieve Myocardial Regeneration (ALLSTAR) (NCT01458405). Available at: http://clinicaltrials.gov/ct2/show/NCT01458405?term=allstar&rank=1.

NIH-PA Author Manuscript

NIH-PA Author Manuscript

NIH-PA Author Manuscript

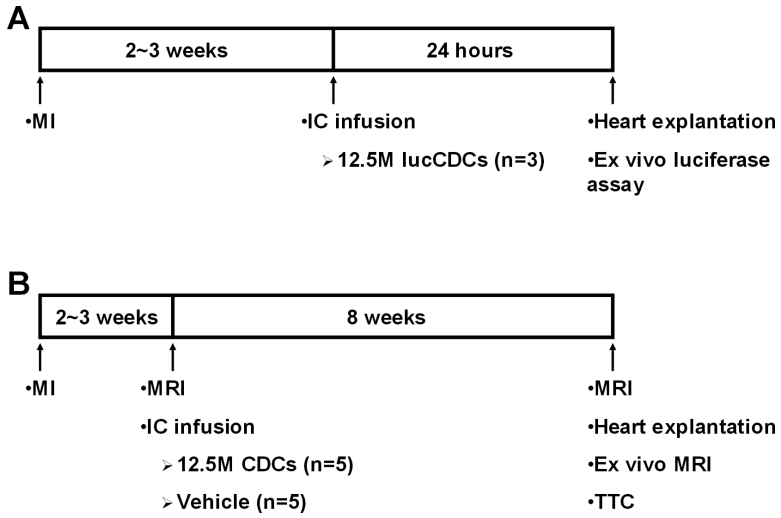

Figure 1.
Study protocol. Schematic depiction of the 24-hour retention study (A) and the validation study (B).

NIH-PA Author Manuscript
NIH-PA Author Manuscript
NIH-PA Author Manuscript

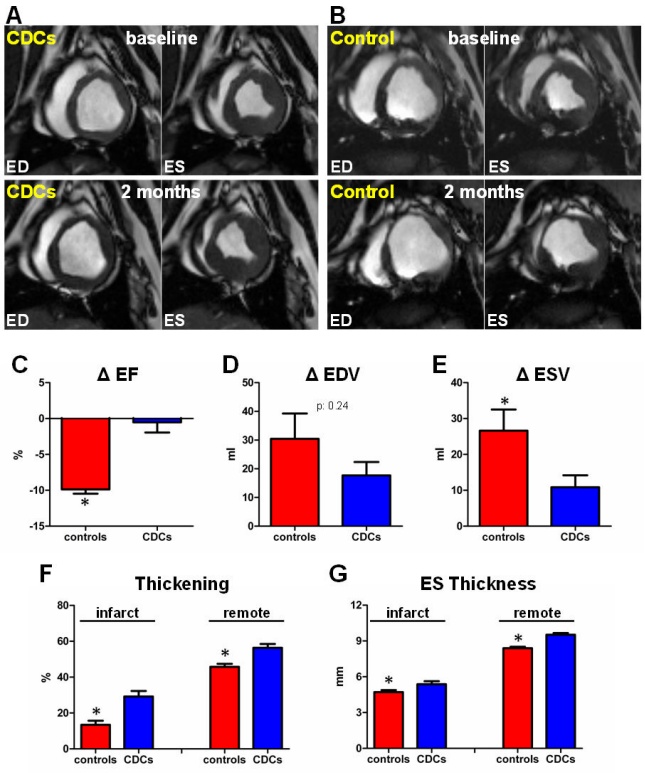

Figure 2.

Allogeneic CDCs attenuate adverse remodeling and improve global and regional function compared to controls. **A,B:** Matched cine short-axis images (at end-diastole [ED] and end-systole [ES]) at baseline and 2 months (videos of the cine acquisitions are provided in the Online Supplement) for a minipig treated with allogeneic CDCs (**A**) and a control minipig (**B**). Images were obtained at similar levels (note the similar morphology of papillary muscles). Changes in ejection fraction (**C**), end-diastolic volume (**D**) and end-systolic volume (**E**) from baseline to 2 months in controls and CDC-treated minipigs. Systolic thickening (**F**) and end-systolic thickness (**G**) in infarcted (infarct) and non-infarcted (remote) segments at 2 months post-infusion in controls and CDC-treated minipigs (* $p<0.05$ vs CDC-treated group).

NIH-PA Author Manuscript

NIH-PA Author Manuscript

NIH-PA Author Manuscript

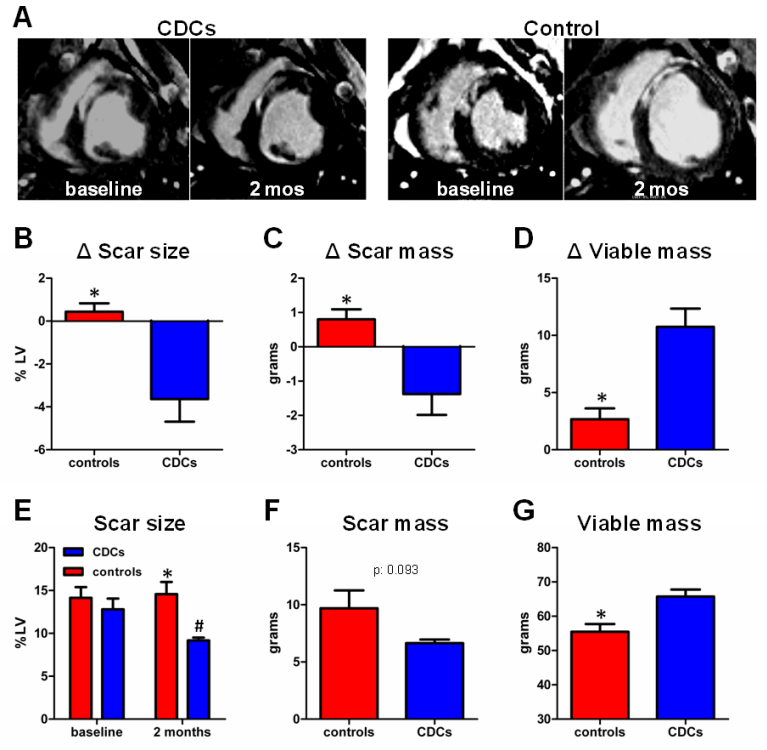

Figure 3.

Allogeneic CDCs decrease scar size, decrease scar mass and increase viable myocardial mass compared to controls, as assessed by MRI. **A:** Representative delayed contrast-enhanced MRI acquisitions of hearts in short-axis section at end-diastole. Scarred myocardium appears white while viable myocardium appears black. In the CDC-treated minipig the scar decreased in transmurality and viable myocardial mass increased over the period of 2 months after CDC infusion. The control minipig was characterized by scar thinning and scar expansion, with no evidence of increase in viable myocardium over the same time period. Changes in scar size (**B**), scar mass (**C**) and viable mass (**D**) from baseline to 2 months in controls and CDC-treated minipigs. **E:** Scar size at baseline and at months post-infusion in control and CDC-treated minipigs. Scar mass (**F**) and viable mass (**G**) at 2 months post-infusion in controls and CDC-treated minipigs (* $p<0.05$ vs CDC-treated group, # $p<0.05$ vs baseline).

NIH-PA Author Manuscript

NIH-PA Author Manuscript

NIH-PA Author Manuscript

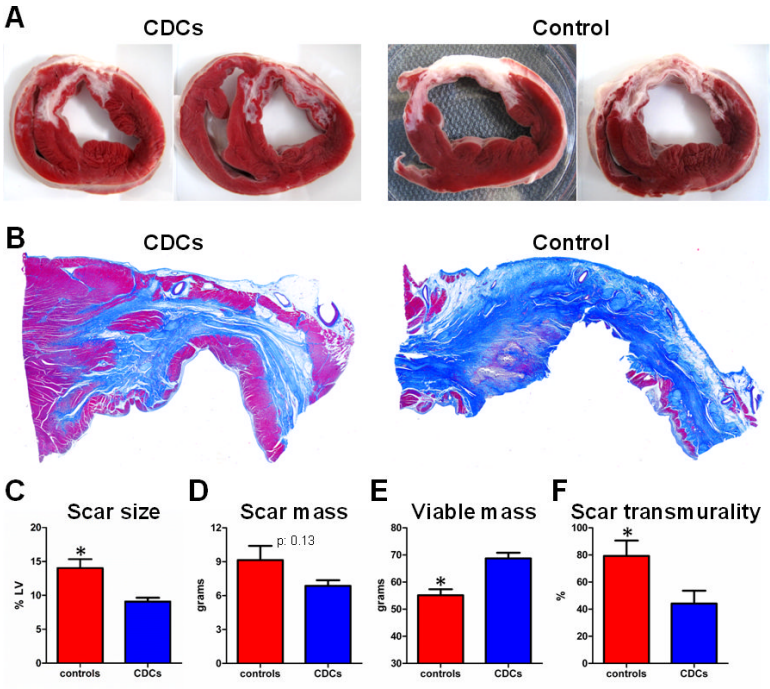

Figure 4.

Allogeneic CDCs decrease scar size and increase viable myocardial mass compared to controls, as assessed by post-mortem histology. **A:** Representative short-axis cardiac slices of 2 CDC-treated and 2 control minipigs at 2 months post-infusion after incubation with TTC. Slices were obtained at similar levels (note the similar morphology of papillary muscles). Viable myocardium stains brick-red, while scarred myocardium appears white (unstained). **B**: Representative sections from the infarcted wall of a treated and a control minipig stained with Masson's trichrome. Viable myocardium stains red, while collagenous scar stains blue. CDC-treated hearts exhibited significant amounts of viable myocardium in the infarcted wall, in the form of endocardial and epicardial muscular layers surrounding the scar and in the form of islets of viable myocardial tissue dispersed in-between the collagen fibers. In control minipigs the scar was largely transmural. Scar size (**C**), scar mass (**D**), viable mass (**E**) and scar transmurality (**F**) at 2 months post-infusion in controls and CDC-treated minipigs, as assessed by post-mortem histology (* $p<0.05$ vs CDC-treated group).

NIH-PA Author Manuscript
NIH-PA Author Manuscript
NIH-PA Author Manuscript

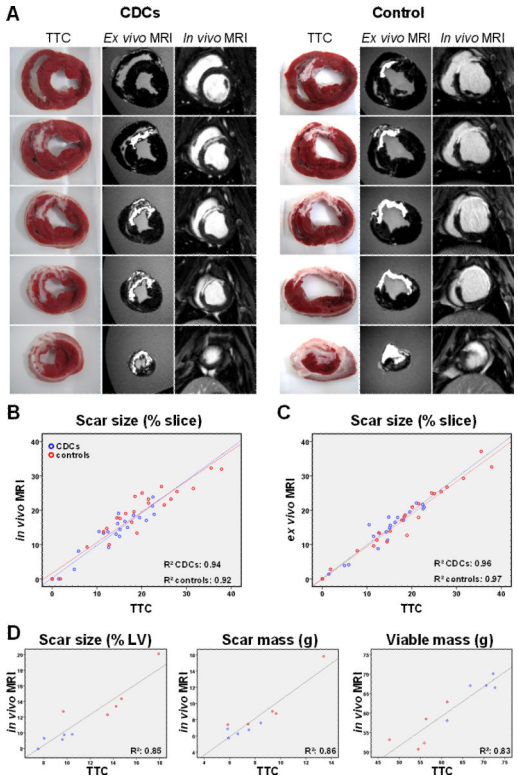

Figure 5.

Comparison of cardiac MRI with histology for assessment of scarred and viable myocardium after cell therapy. **A:** TTC-stained cardiac slices matched with their corresponding delayed contrast-enhanced MRI images (from both the in vivo and ex vivo MRI datasets) for a CDC-treated and a control minipig. Areas of hyperenhancement in cardiac MRIs correspond excellently to regions of scarred myocardium in histological slices. The treated minipig MRI demonstrates endocardial and epicardial rims of non-hyperenhanced tissue in the infarcted wall which correspond excellently to endocardial and epicardial TTC-positive muscular layers surrounding the scar in histological slices. The control heart is characterized by a transmural scar, and no viable myocardium can be detected in the infarct area by either MRI or histology. Correlation of MRI measurements of scar size as % of isolated cardiac slices (for in vivo [**B**] and ex vivo [**C**] MRI), scar size as % of LV, LV scar mass and LV viable mass (**D**) with the corresponding histological measurements.

NIH-PA Author Manuscript

NIH-PA Author Manuscript

NIH-PA Author Manuscript

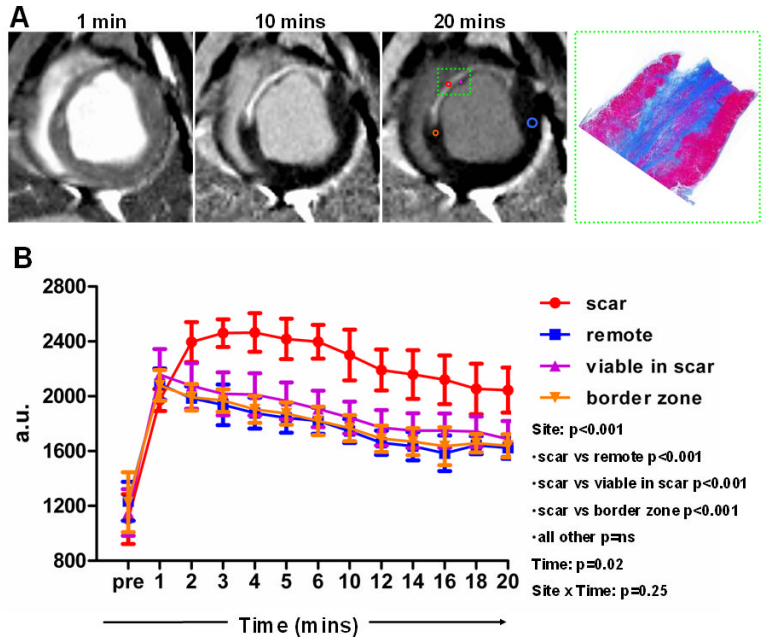

Figure 6.

Gd-contrast myocardial kinetics in cell-treated hearts. **A:** A series of dynamic delayed contrast enhancement images with a fixed T1 were acquired and signal intensity of specific areas (collagenous scar, viable myocardium in the infarcted region, viable myocardium at the border zone, remote myocardium) was measured at various timepoints following contrast administration, resulting in the generation of site-specific Gd-contrast curves in all cell-treated minipigs. **B**: Gd-contrast kinetics pooled data from all treated minipigs. Analysis using a linear mixed effects model demonstrated that Gd-contrast kinetics were identical in cell-treated viable (non-hyperenhanced) areas and in the remote non-cell treated healthy myocardium. Image on the right in A is the corresponding histological section stained with Masson's trichrome of the inset in the MRI acquisitions.

NIH-PA Author Manuscript
NIH-PA Author Manuscript
NIH-PA Author Manuscript

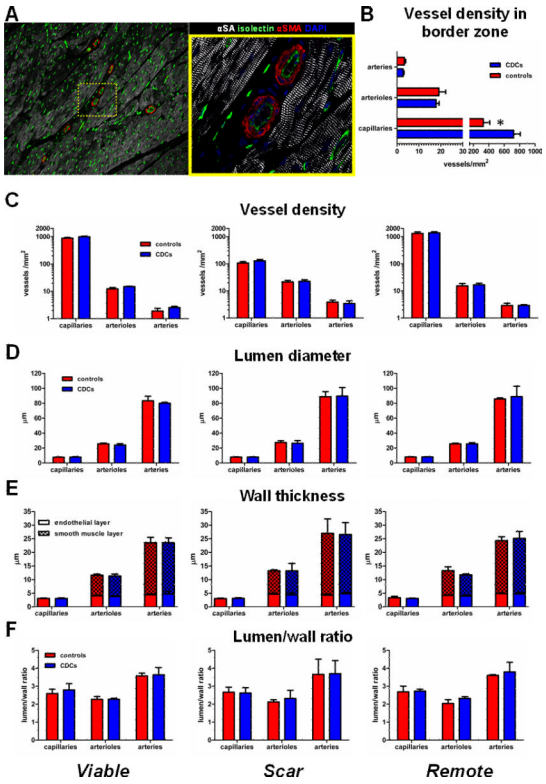

Figure 7.

Vessel density and architecture. **A:** Vascular density and architecture were evaluated by immunostaining for α-sarcomeric actinin, α-smooth muscle actin and isolectin. Image on the right is a high-power image of inset on left. **B:** Vessel density in the border zone (defined as the region at the edges of the scar comprising areas of both scarred and viable myocardium). Vessel density (**C**), lumen diameter (**D**), total wall thickness, endothelial layer thickness, smooth muscle layer thickness (**E**) and lumen to wall ratio (**F**) in viable myocardium in the infarcted wall (viable), in the collagenous scar (scar) and in the remote non-infarcted myocardium (remote) (* $p<0.05$ vs CDC-treated group).

NIH-PA Author Manuscript
NIH-PA Author Manuscript
NIH-PA Author Manuscript

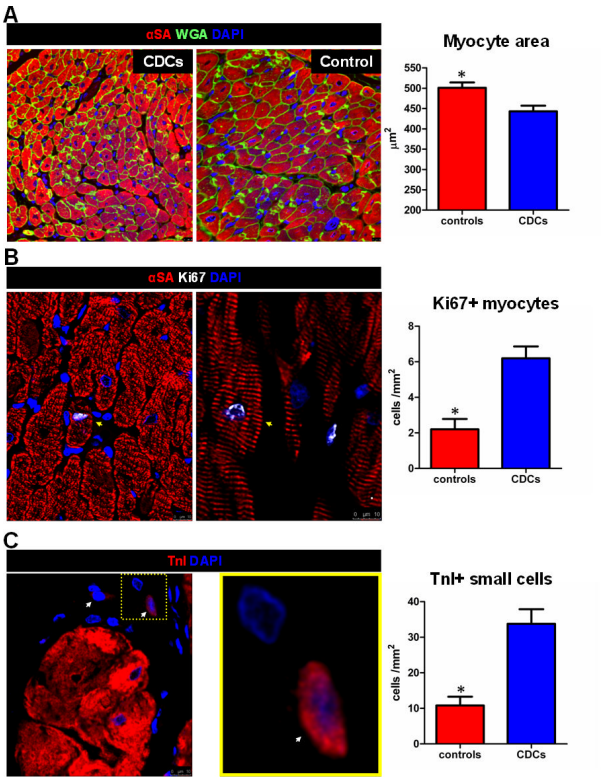

Figure 8.

Allogeneic CDCs attenuate myocyte hypertrophy and promote endogenous regeneration in the infarct and peri-infarct area. **A:** Cardiomyocyte cross-sectional area in the infarct and peri-infarct area. **B:** Cycling cardiomyocytes (arrows) in the infarct and peri-infarct area. **C:** Small TnI+ cells (arrows; image on the right is a magnification of the inset on left) in the infarct and peri-infarct area (* $p<0.05$ vs CDC-treated group).